BES Analysis Memo
Search for $\psi(2S)$ Decays to Vector plus Tensor Mesons

Li Xinhua
email: LIXH@bepc5.ihep.ac.cn
(Revised Nov. 6, 1997)

Abstract

The hadronic decays $\psi(2S) \to \omega f_2$, ρa_2, $K^{*0}K_2^{*0}$ and $\phi f_2'(1525)$ have been studied in a sample of 3.7×10^6 $\psi(2S)$ events. Measurements of their branching fractions are presented. All channels violate the "15% *rule*" predicted by perturbative QCD compared with the corresponding J/ψ decays. As vector-tensor pair combinations, they provide the first anomalous example of non-vector-pseudoscalar decays of charmonium.

I. INTRODUCTION

There exists a long standing puzzle in the study of charmonium decays. According to Applequist and Politzer [1], there is a direct parallel between the decay of $\psi(2S)$ and J/ψ to three massless gluons

$$Q_h \equiv \frac{B(\psi(2S) \to ggg)}{B(J/\psi \to ggg)} = \frac{B(\psi(2S) \to e^+e^-)}{B(J/\psi \to e^+e^-)} = (14.6 \pm 2.2)\%$$

where the leptonic branching fractions from PDG [2] are used.

The Mark II first revealed unexpected small values for the ratios of $\psi(2S)$ to J/ψ branching fractions for decays to $\rho\pi$ and $K^{*\pm}K^{\mp}$. With a data sample of 1.02×10^6 produced $\psi(2S)$ events, it was found that $Q_{\rho\pi} < 0.63\%$ (90% $C.L.$) and $Q_{K^{*\pm}K^{\mp}} < 2.07\%$ (90% C.L.) [3].

Following Mark II, several radiative decays were measured by the Crystal Ball experiment [4]. Radiative decays of $\psi(2S)$ to the tensor f_2 was observed but neither to the η nor the η'. These results, in combination with the Mark II results, immediately led to a conclusion that the suppressed modes are just vector-pseudoscalar decays of $\psi(2S)$. Ever since it becomes popular in the literature to refer to the puzzle as "$vector - pseudoscalar\ puzzle$".

A number of theoretical models [5] have been suggested to explain the puzzle, but none of them are satisfactory.

This paper extends observation to the vector-tensor combination decays, $\psi(2S) \to \omega f_2$, ρa_2, $K^{*0}K_2^{*0}$ and $\phi f_2'$. Data were taken during 1993-1995 at the BEPC and reconstructed in version 86. The total event number of $\psi(2S)$ is $(3.7 \pm 0.3) \times 10^6$ got by observing the inclusive production of J/ψ in the process $\psi(2S) \to \pi^+\pi^-J/\psi$ and using the branching fraction of $\psi(2S) \to \pi^+\pi^-J/\psi$ of PDG [2]. C.Z.Yuan has also analyzed two decay channels, $\psi(2S) \to K^{*0}K_2^{*0}$ and $\phi f_2'$, with the same data samples which reconstruction was in version 85 for 1993/94 data and in version 86 for 1995 data. His observation results are listed in this memo for reference [6] [7].

II. $\psi(2S) \to \pi^+\pi^-\pi^+\pi^-\pi^0$ SELECTION

Events with four charged tracks (MFIT=2) in the polar angle region $-0.8 < \cos\theta < 0.8$ and with zero net charge have been selected. Moreover, at least two neutral tracks with polar angle $-0.75 < \cos\theta < 0.75$ and also not hitting the central ribbon range ($Z_{sc} < -4cm$ or $Z_{sc} > 4cm$) are required for photon candidates.

Magnetic field correction is made to the momentum of charged track. Momentum corrections are further made for energy loss and multiple Coulomb scattering in the material before charged particles enter the drift volume in BES inner detector. So are photon directions entering shower counter for beam position dispersion in the colliding zone.

Events are kinematically $4C2\gamma$ fitted with all pairs of photon candidates. The pair with highest probability of fit are selected and it is also required to be greater than 0.01. The π^0 is selected by requiring the invariant mass of two photons to be $85 < M_{\gamma\gamma} < 205\ MeV$. Its side band is defined as the mass range $40 < M_{\gamma\gamma} < 80\ MeV$ and $210 < M_{\gamma\gamma} < 290\ MeV$. Several steps are processed to remove fake photon contamination. The angle between photon and charged track is larger than 13^o. The distance between photon and charged track hitting shower counter is larger than 35cm. The fitted energy of photon is higher than 60MeV. Figure 1 shows the fitted photon energy spectrum (2 entries/event) and the $M_{\gamma\gamma}$ vs E_{min} (the minimum energy of two photons, 1 entry/event). Figure 2 presents the $M(\gamma\gamma)$ before, after, or removed by the cut (fitted photon energy >60MeV).

Furthermore, the J/ψ contamination of e^+e^- or $\mu^+\mu^-$ from $\psi(2S) \to \eta J/\psi$ where η decays to $\pi^+\pi^-\pi^0$ and J/ψ decays to leptons is removed by $M(\pi^+\pi^-) < 2.9\ GeV/c^2$. Figure 3 shows $M(\pi^+\pi^-)$ plot (4 entries/event) removed by or after this cut.

The dE/dx measurements are used to select pion tracks with confidence level larger than 0.003 for each track and 0.01 for all tracks combined. So are the TOF measurements when hit qualities are good ($T_{qual} = 1$) (at least one track with $T_{qual} = 1$ is required in the event selection). Figure 4 shows ($M_{\gamma\gamma}$) spectrum for the events surviving all the above selections. The π^0 mass resolution is 14MeV. Figure 5 presents the simulated π^0 mass plot of $\psi' \to \omega\pi^+\pi^-$. Both in data and Monte Carlo, the higher side of π^0 mass spectrum should be wider than the lower side because of larger energy resolution. Supposing $\sigma_E/E = 25\%/\sqrt{E}$, σ_E gets larger when E increases as higher $M(\gamma\gamma)$. Therefore a single Gaussian curve fit to π^0 mass plot does not work well in both data and Monte Carlo.

No $\pi^+\pi^-$ combination is allowed to recoil to J/ψ within $50MeV/c^2$ of J/ψ mass to exclude the background $\psi(2S) \to \pi^+\pi^- J/\psi$ with J/ψ decaying to $\pi^+\pi^-\pi^0$. Figure 6 shows $M(\pi^+\pi^-\pi^0)$ plot (4 entries/event) for the events removed by or after this rejection.

The effects of the various selection cuts on the data are summarized in Table 1. Included in the table are the results that obtained when the same analysis is applied to samples of Monte Carlo simulated events $\psi(2S) \to \omega\pi^+\pi^-$, ωf_2 and ρa_2.

Table 1. A tabulation of the $\psi(2S) \to 2(\pi^+\pi^-)\pi^0$ selection cuts.

a). Samples of $\omega\pi^+\pi^-$, ωf_2 and ρa_2 are the Monte Carlo simulated events;
b). The MDC cut is Nchrg=4, $\sum_i q = 0$ and $|\cos\theta| < 0.8$;
c) 141 events survive the ω selection when $CL(TOF)$ is not applied to the data.

	data	$\omega\pi^+\pi^-$	ωf_2	ρa_2
Generated		12000	12000	19200
MDC	440698	4566	4751	7037
$N_\gamma > 1$	359933	2324	2490	4066
$CL(4C) > 0.01$	23489	1712	1824	2932
$\cos\theta_{\gamma ch} < 0.975$	15990	1448	1508	2841
$d_{\gamma ch} > 35cm$	14605	1307	1347	2769
$E_\gamma^{fit} > 60MeV$	12225	1041	1101	2442
$m_{\pi^+\pi^-} < 2.9GeV$	11934	1038	1099	2439
$CL(dE/dx) > 0.01$	9519	998	1060	2356
$CL(TOF) > 0.01$	8547	966	1033	2325
Remove $\pi^+\pi^- J/\psi$	1206	920	1011	2230
$85 < m_{\gamma\gamma} < 205MeV$	939	914	997	2197
Select ω	128	834	912	
Select $\rho^0\rho^\pm\pi^\mp$	301			1535

III. ANALYSIS OF $\psi(2S) \to \omega\pi^+\pi^-$

The $\pi^+\pi^-\pi^0$ mass spectrum (figure 7) shows significant ω signal. The similar plot of π^0 side band (figure 8) shows invisible ω signal. The mass distribution is fitted to a Breit-Wigner curve with width fixed to PDG [2] and float mass added to a quaduatical background. Mass resolution is 13.4 MeV got from simulation and 10.4 ± 1.5 MeV from data. Figure 9 shows the unbinned fit plot of data. The fit quality is $\chi^2 = 43.36/35 dof$. It gives 114.0 ± 12 events and mass of ω $(781.7 \pm 2.0) MeV/c^2$ well consistent with PDG [2]. Figure 10 is the corresponding fit plot of Monte Carlo simulation. The efficiency is 0.079 calculated by Monte Carlo simulation with uniform phase space distribution. The branching fraction is obtained

$$B(\psi(2S) \to \omega\pi^+\pi^-) = (4.6 \pm 0.5 \pm 0.9) \times 10^{-4},$$

where the first error is statistical and second systematic. The systematic error (sum up 20%) results from efficiency simulation (semi-arbitrary but conservative assigned 15%), total number of $\psi(2S)$ (10%), $B(\omega \to \pi^+\pi^-\pi^0)$ in PDG [2] (0.8%), kinematic fits (7%), π^0 mass band selection (4%) and other event selections (5%).

The $\omega\pi^+\pi^-$ candidates are selected by requiring $740 < m_{\pi^+\pi^-\pi^0} < 820\ MeV/c^2$. $680 < m_{\pi^+\pi^-\pi^0} < 720 MeV/c^2$ and $840 < m_{\pi^+\pi^-\pi^0} < 880 MeV/c^2$ are chosen for the ω side band. The Dalitz plot of $\omega\pi^+$ versus $\omega\pi^-$ are in figure 11 for ω mass region and figure 12 for the side band.

The $\omega\pi^\pm$ mass spectrum figure 13 shows a clear $b_1^\pm$ signal owing to the proximity to the phase space limit. The similar plot for the ω side band figure 14 shows very few $b_1^\pm$ signals. The mode $b_1^\pm\pi^\mp$ will not analyzed further in this note. We are looking forward to Hawaii's result.

The decay $\psi(2S) \to \omega f_2$ is investigated on the $\pi^+\pi^-$ mass plot recoiling to the ω mass band (figure 16) and also to the ω side band (figure 15). The $f_2(1270)$ signal is invisible on both plots. It has been fitted to a Breit-Wigner curve with width and mass fixed to PDG [2] added to quadratic background (the fit to linear background curve makes no difference). Mass resolution is 12.3 MeV got by simulation. The fit leads to 8.8 ± 9.2 events. At the 90% confidence level the event number is less than 23.8. The fit quality is $\chi^2 = 66.56/51\ dof$. The fit plot is shown in figure 16. The corresponding fit plot of Monte Carlo is in figure 17. The efficiency is 0.074 calculated by simulation with uniform phase space distribution. Considering an isospin ratio 2:1 for f_2 decays into $\pi^+\pi^-$ or $\pi^0\pi^0$, one gets the branching fraction

$$B(\psi(2S) \to \omega f_2) < 1.8 \times 10^{-4} \qquad \text{(C.L.=90\%)}$$

IV. ANALYSIS OF $\psi(2S) \to \rho A_2$

The events with $742 < m(\pi^+\pi^-\pi^0) < 822 MeV/c^2$ are rejected as background channel $\psi(2S) \to \omega\pi^+\pi^-$. The channel ρa_2 is analyzed in $\rho^0\rho^\pm\pi^\mp$ combination which decays to $\pi^+\pi^-\pi^+\pi^-\pi^0$ final state. The $\rho^0\rho^\pm\pi^\mp$ candidate is selected by minimizing a quantity

$$\Delta = \sqrt{(m_{\pi^+\pi^-} - m_{\rho^0})^2 + (m_{\pi^0\pi^\pm} - m_{\rho^\pm})^2}.$$

and a cut $\Delta_{min} < 200\ MeV/c^2$ is applied. The Δ_{min} plot is shown on Figure 18 for data, and Figure 19 for Monte Carlo, respectively. The resolution of the Δ_{min} quantity is shown on figure 20 where the widths of $\rho^\pm$ and ρ^0 are set to zero in the event generation of $\psi(2S) \to \rho a_2 \to \rho^0\rho^\pm\pi^\mp$. The $a_2(1320)$ signal is very marginal on the combining $\rho^0\pi^\pm$ and $\rho^\pm\pi^\mp$ mass plot from $\rho^0\rho^\pm\pi^\mp$ candidate event (figure 21). The a_2 mass resolution is 10.3 MeV got from simulation. A fit to a Breit-Wigner curve with a_2 mass and width fixed to PDG [2] over a quadratic background yields ρa_2 event number 3.9 ± 15.7. The event number is less than 29.6 at 90% confidence level. The fit quality is $\chi^2 = 53.41/56\ dof$. Simulation with uniform phase space distribution gives 0.074 detection efficiency (figure 22). Assuming an isospin ratio of $a_2^+\rho^- : a_2^-\rho^+ : a_2^0\rho^0 = 1 : 1 : 1$ for $\psi(2S)$ decay, one calculates

$$B(\psi(2S) \to \rho a_2) < 2.5 \times 10^{-4} \qquad \text{(C.L.=90\%)}.$$

V. ANALYSIS OF $\psi(2S) \to \pi^+\pi^-K^+K^-$

Four charged track net charge zero events have been selected if each track with high quality in track fitting (MFIT=2) and polar angle in the region $|\cos\theta| < 0.8$. Magnetic field correction is made to momentum of charged track. Momentum correction is further made for energy loss and multiple Coulomb scattering in the material before track enters the drift volume in BES inner detector. Events are kinematic fitted to $\psi(2S) \to \pi^+\pi^-K^+K^-$. In order to get better separation among different track assignment (4 assignments of π^+, π^-, K^+, K^- track / per event), we combine TOF, dE/dx and kinematic fit to get a combined probability for an assignment. The combined χ^2 is calculated as:

$$\chi^2 = \sum_i \chi^2(TOF) + \sum_i \chi^2(dE/dx) + \chi^2(4C\_fits).$$

Similarly calculated the combined degrees of freedom. The track assignment with highest combined probability is selected as $\pi^+\pi^-K^+K^-$ candidate among four assignments. The probability of kinematic fit is also required to be larger than 0.01. The plot (figure 23) of $\pi^+\pi^-$ recoiling mass which is calculated using the reconstructed track momentum shows a contamination of $\psi(2S) \to \pi^+\pi^-J/\psi$ with J/ψ decaying to lepton pair. Thus the $\pi^+\pi^-$ recoiling mass is required to be lower than 3.0 GeV or higher than 3.2 GeV to exclude it. Figure 24 shows the confidence level of dE/dx and TOF measurement. The dE/dx measurements are used to select π and K tracks with confidence level larger than 0.003 for each track and 0.01 for all tracks combined. So are the TOF measurements when the hit qualities are good ($T_{qual} = 1$) ($T_{qual} = 1$ for at least one track per event is required). $R = E_{sc}/P$ is defined in order to remove electron. Any track with $P > 1GeV/c$ and $R > 1$ is removed as electron; Any pair of positive and negative tracks with both track $P > 1GeV/c$ and $(R_+ - 1)^2 + (R_- - 1)^2 < 0.36$ are removed. In order to remove μ, $D^2 = (x_{proj} - x_{hit})^2 + (y_{proj} - y_{hit})^2$ is defined. $D < 4cm$ is taken as 1st layer μ counter hit, $D < 5cm$ as 2nd layer μ counter hit, and $D < 6cm$ as 3rd layer μ counter hit. Any pair of positive and negative tracks with (0,3), (1,2), (2,2), (2,3) or (3,3) μ counter hits are removed as muons. K^{*0} is selected by $800 < m(k^{\pm}\pi^{\mp}) < 1000\ MeV/c^2$. $680 < m(k^{\pm}\pi^{\mp}) < 780\ MeV/c^2$ and $1020 < m(k^{\pm}\pi^{\mp}) < 1120\ MeV/c^2$ are selected as the side band. The resulting plots are in figure 25, the upper left is the scatter plot of $K^+\pi^-$ vs $K^-\pi^+$; the lower left the mass of $K^{\pm}\pi^{\mp}$; the upper right $m(K^{\pm}\pi^{\mp})$ recoiling to K^{*0}; the lower right $m(K^{\pm}\pi^{\mp})$ recoiling to K^{*0} side band.

The effects of the various selection cuts on the data $\psi(2S) \to \pi^+\pi^-K^+K^-$ are summarized in Table 2. Included in the table are the results that obtained when the same analysis is applied to samples of Monte Carlo simulated events $\psi(2S) \to K^{*0}K_2^{*0}$.

On $M(k^+k^-)$ plot of data, there are around 60 ϕ signals which are from $\psi(2S) \to \phi\pi^+\pi^-$. However, its contamination is negligible. Producing 10000 events of $\psi(2S) \to \phi\pi^+\pi^-$ with HOWL generator, There are 4438 entries on $M(k^{\pm}\pi^{\mp})$ mass plot. On the interested $M(k^{\pm}\pi^{\mp})$ plot recoiling to k^{*0}, there are 442 entries with $M(k^{\pm}\pi^{\mp})$ mostly lower than 900MeV or higher than 1600MeV. Therefore its contamination into $k^{*0}k_2^{*0}$ is not a problem (see figure 26).

The mass plot of $K^{\pm}\pi^{\mp}$ recoiling to K^{*0} is fitted with two Breit-Wigner curves of K^{*0} and K_2^{*0} over a quadratic background (figure 27). Monte Carlo simulation gives mass resolutions 4.9 MeV for the K^{*0} and 6.7 MeV for the K_2^{*0}. The mass and width of K_2^{*0} are set to PDG. So is the width of K^{*0}. The fit quality is $\chi^2 = 71.18/59\ dof$. The fit yields mass of K^{*0} $890.7 \pm 5.4\ MeV$, K^{*0} number 53.8 ± 10.3, and K_2^{*0} number 1.4 ± 8.6. At the 90% confidence level, the number of K_2^{*0} is less than 17.2. The efficiency is 17.1% calculated by simulation with uniform phase space distribution (figure 28). Applying $K^{\pm}\pi^{\mp} : K^0\pi^0 = 2:1$ for both K^{*0} and K_2^{*0} decay, one gets

$$B(\psi(2S) \to K^{*0}K_2^{*0}) < 1.4 \times 10^{-4} \qquad (C.L. = 90\%).$$

Changzheng Yuan has also analyzed the above decay channel and got an upper limit of the branching fraction [6]

$$B(\psi(2S) \to K^{*0}K_2^{*0}) < 1.79 \times 10^{-4} \qquad (C.L. = 90\%)$$

VI. ANALYSIS OF $\psi(2S) \to K^+K^-K^+K^-$

Events with four charged tracks (MFIT=2) in the polar angle region $-0.8 < \cos\theta < 0.8$ and with zero net charge have been selected. Magnetic field correction is made to momentum of charged track. Momentum correction is further made for energy loss and multiple Coulomb scattering in the material before track enters the drift volume in BES inner detector. Events are kinematically $4C$ fitted to improve mass resolution and exclude background. The probability of fit is required to be higher than 0.01. Figure 29 shows the confidence level of dE/dx and TOF measurement of the surviving events. The dE/dx measurements are used to select kaon tracks with confidence level larger than 0.003 for each track and 0.01 for all tracks combined. So are the TOF measurements when hit qualities are good ($T_{qual} = 1$) (at least one track with $T_{qual} = 1$ is required in the event selection). The electrons and muons are rejected by the procedure of Section V. There remains 41 events after the above selections. The effects of the various selection cuts on the data are summarized in Table 2. Included in the table are the results that obtained when the same analysis is applied to the Monte Carlo simulated $\phi f_2'$ events.

The resulting dalitz plot (figure 30, 1 entry/event) seems to show ϕ signal band. The ϕ mass resolution is 4.1 MeV from Monte Carlo, 5.7$\pm$1.1 MeV from data. Figure 31 is the mass plot of K^+K^- (4 entries/event). The ϕ candidate is selected as $m_{K^+K^-} < 1040\ MeV/c^2$ to investigate the recoiling part. The mass plot of K^+K^- pair recoiling to ϕ (figure 32) shows ϕ signal but $f_2'(1525)$ is marginal. Two events with double counting (2 entries/event) are in the ϕ mass range ($m_{K^+K^-} < 1040\ MeV/c^2$). Based on these two events, the number of $\phi\phi$ events is less than 5.32 at the 90% confidence level. The PDG reports the mass 1525 ± 5 MeV and width 76 ± 10 MeV for the f_2' meson. Simulation gives the mass resolution 6 MeV. There are 3 events on figure 32 that fall into one width region around the f_2' mass. Taken all of them as f_2' candidates, at the 90% confidence level the number is less than 6.68. Fit to f_2' mass plot in Monte Carlo using Breit-Wigner curve with linear background shape and 6MeV fixed mass resolution results in the followings: $\chi^2 = 186.97/134$, f_2' mass $1525.7 \pm 1.4 MeV$, width $73.2 \pm 3.1 MeV$, and efficiency 0.181 for $\psi' \rightarrow \phi f_2'(1525)$. The branching fractions are calculated

$$B(\psi(2S) \rightarrow \phi f_2'(1525)) < 4.7 \times 10^{-5} \qquad \text{(C.L.=90\%)}.$$

Changzheng Yuan has also observed the decay $\psi(2S) \rightarrow \phi f_2'(1525))$ and got an upper limit [7]

$$B(\psi(2S) \rightarrow \phi f_2'(1525)) < 5.3 \times 10^{-5} \qquad \text{(C.L.=90\%)}.$$

VII. SUMMARY AND DISCUSSION

The decays of $\psi(2S)$ to $2(\pi^+\pi^-)\pi^0$, $\pi^+\pi^-K^+K^-$ and $K^+K^-K^+K^-$ have been studied from a high statistics constrained and fully reconstructed events. Four vector-tensor combinations, ωf_2, ρa_2, $K^{*0}K_2^{*0}$ and $\phi f_2'(1525)$ are measured in $\psi(2S)$ decays. Table 3 summarizes the results of branching ratios measured for $\psi(2S)$ decays into vector plus tensor combinations and also the PDG [2] values for the corresponding J/ψ decays. The ratio of the branching fraction of $\psi(2S)$ decays to J/ψ are also listed in the table except for the channel $\phi f_2'$ which branching fraction is poorly measured. All channels, except for $\phi f_2'$, give values of the ratio of branching fractions of the $\psi(2S)$ to the J/ψ much lower than the prediction of perturbative QCD. As vector-tensor combinations, their suppressions provide a striking deviation from the expectation [1] and as yet there is no satisfactory theoretical explanation.

Table 2. A tabulation of the $\psi(2S) \to \pi^+\pi^-K^+K^-$ and $K^+K^-K^+K^-$ selection cuts.

a). Samples of $K^{*0}K_2^{*0}$ and $\phi f_2'$ are the Monte Carlo simulated events;
b). The MDC cut is Nchrg=4, $\sum_i q = 0$ and $|\cos\theta| < 0.8$;
c). The $\pi^+\pi^-J/\psi$ cut is not applied to $K^+K^-K^+K^-$ and $\phi f_2'$.

	$\pi^+\pi^-K^+K^-$	$K^+K^-K^+K^-$	$K^{*0}K_2^{*0}$	$\phi f_2'$
Generated			14800	6000
MDC	440698	440698	5310	1837
$CL(4C) > 0.01$	3460	664	4000	1172
$CL(dE/dx) > 0.01$	2389	42	3878	1163
$CL(TOF) > 0.01$	2082	41	3704	1075
Remove electron	2068	41	3702	1075
Remove $\pi^+\pi^-J/\psi$	624		3619	
Remove muon	614	41	3618	1075

Table 3 Experimental ratios of $\psi(2S)$ compared to J/ψ (limits at 90% confidence level).

	$B(\psi(2S))$	$B(J/\psi)$	$B(\psi(2S))/B(J/\psi)$
$\omega\pi^+\pi^-$	$(4.6 \pm 0.5 \pm 0.9) \times 10^{-4}$	$(7.2 \pm 1.0) \times 10^{-3}$	0.064 ± 0.015
ωf_2	$< 1.8 \times 10^{-4}$	$(4.3 \pm 0.6) \times 10^{-3}$	< 0.042
ρa_2	$< 2.5 \times 10^{-4}$	$(10.9 \pm 2.2) \times 10^{-3}$	< 0.023
$K^{*0}K_2^{*0} + c.c.$	$< 1.4 \times 10^{-4}$	$(6.7 \pm 2.6) \times 10^{-3}$	< 0.022
$\phi f_2'$	$< 4.7 \times 10^{-5}$	$(8 \pm 4) \times 10^{-4}$	

REFERENCES

[1] T. Applequist and D. Politzer, Phys. Rev. Lett. 34, 43(1975).
[2] R.M.Barnett et al. (Particle Data Group), Phys. Rev. D54, 1(1996).
[3] M.E.B.Franklin et al., Phys. Rev. Lett. 51, 963(1983).
[4] R.A.Lee, SLAC-PUB-3676, May 1985.
[5] G.Karl and W.Roberts, Phys. Lett. B144, 263(1984);
G.Karl and S.F.Tuan, Phys. Rev. D34, 1629(1986);
M.Chaichian et al., Nucl. Phys. B323, 75(1989);
S.S.Pinsky, Phys. Lett. B236, 479(1990);
W.S.Hou and A.Soni, Phys. Rev. Lett. 50, 569(1983);
S.J.Brodsky et al., Phys. Rev. Lett. 59, 621(1987);
X.Q.Li et al., Phys. Rev. D55, (1997) 1241;
S.J.Brodsky and M.Karliner, Phys. Rev. Lett. 78, 4682(1997).
[6] C.Z. Yuan, $\psi(2S) \to \pi^+\pi^- K^+K^-$, BES analysis memo, 1996.
[7] C.Z. Yuan, $\psi(2S) \to 2(K^+K^-)$, BES analysis memo, 1995.

FIGURES

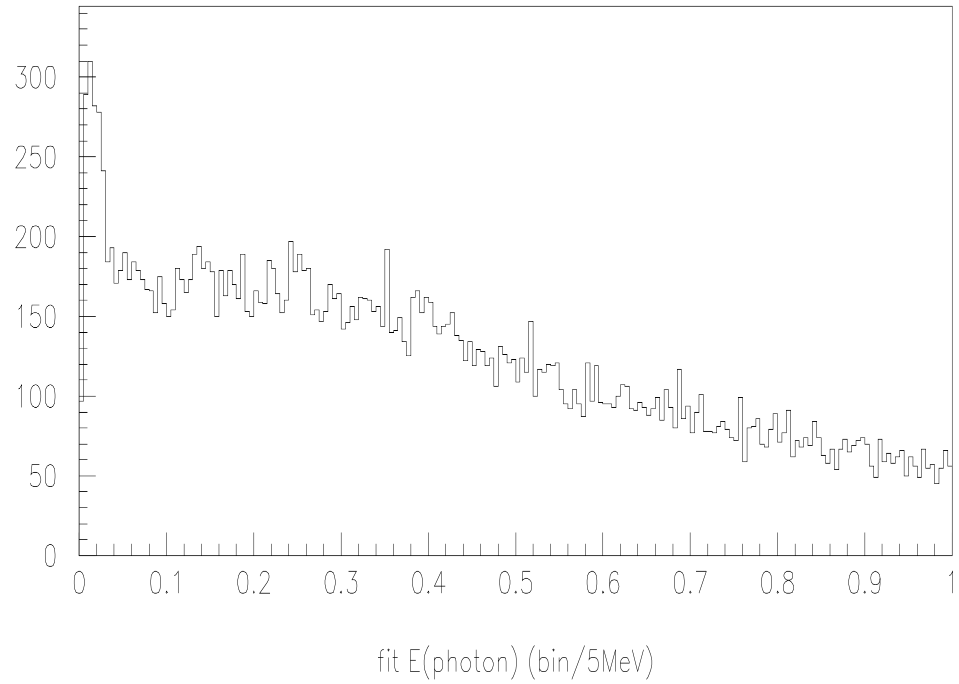

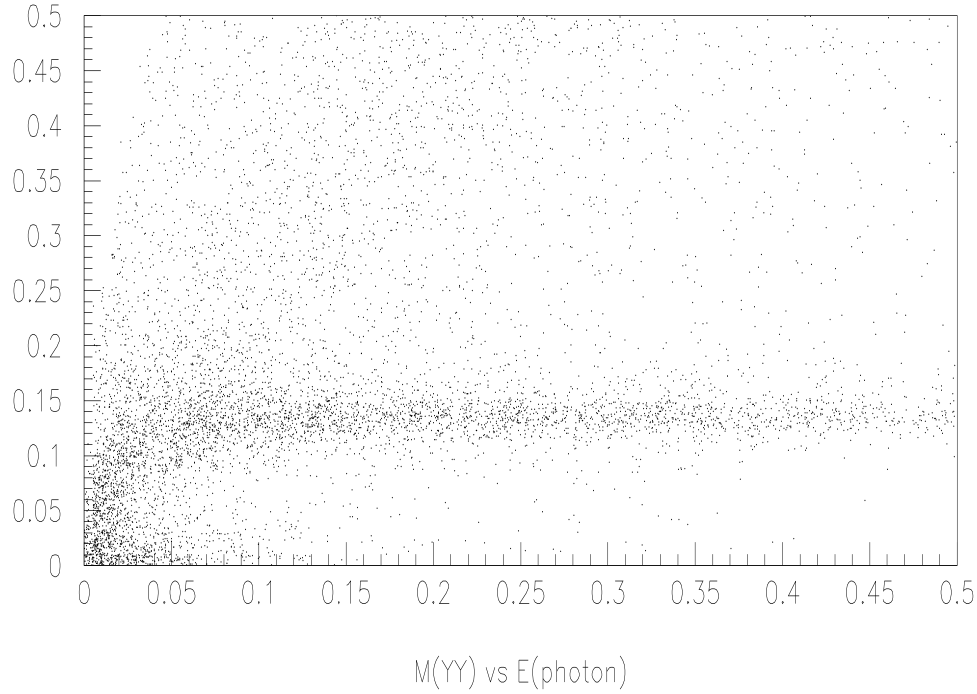

FIG. 1. Fitted photon energy spectrum of data

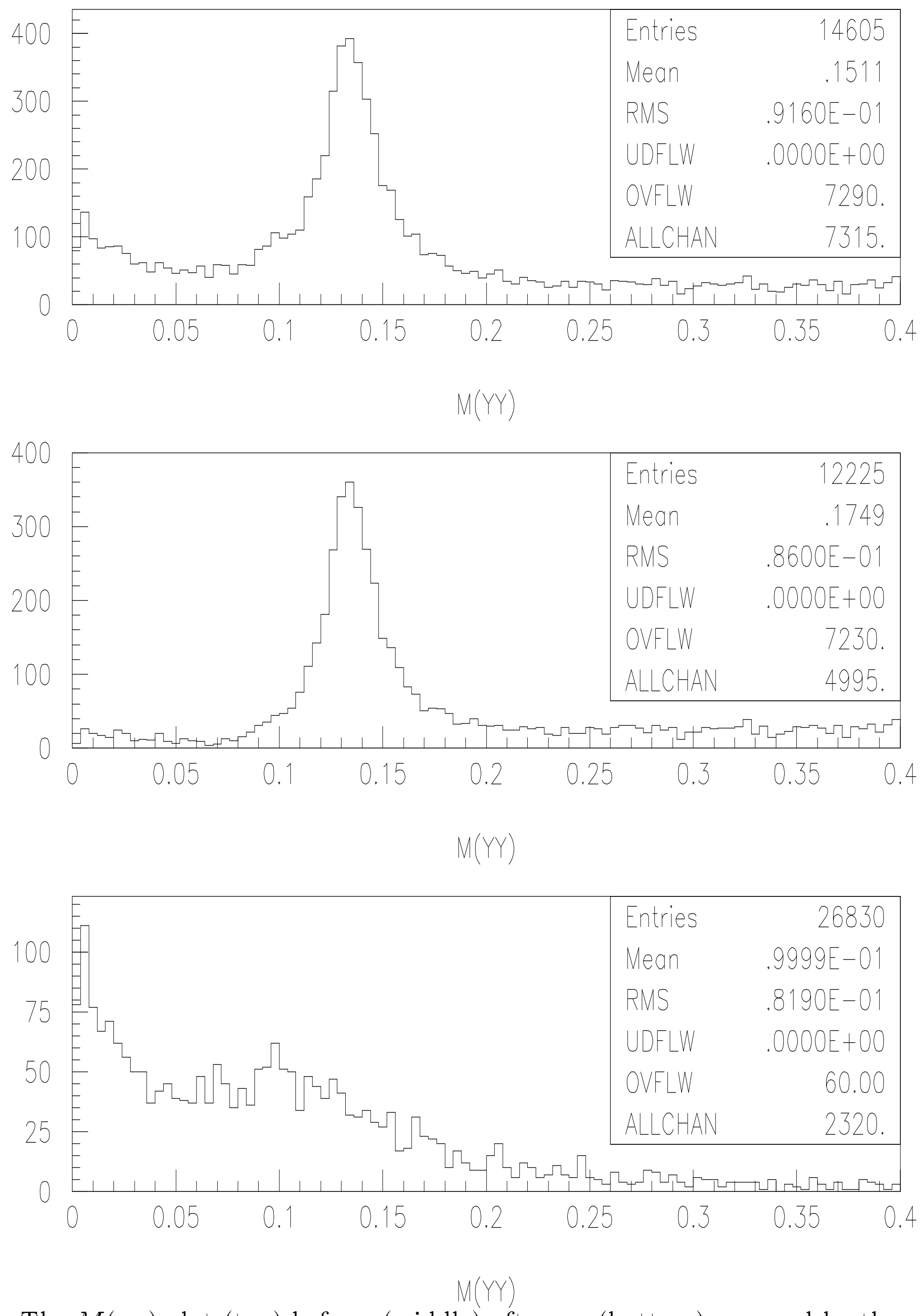

FIG. 2. The $M(\gamma\gamma)$ plot (top) before, (middle) after, or (bottom) removed by the cut of fitted $E_\gamma > 60MeV$

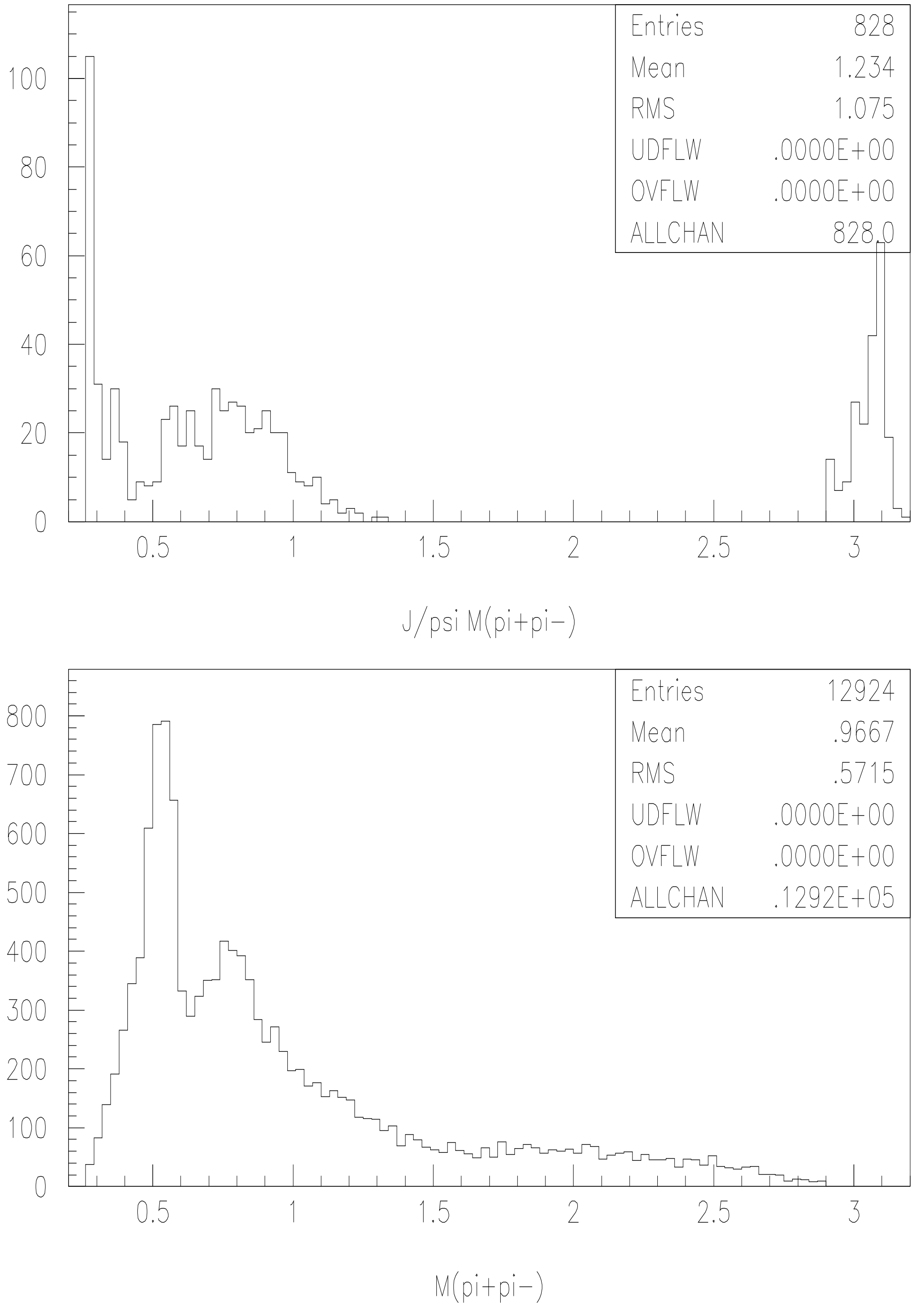

FIG. 3. The $M(\pi^+\pi^-)$ plot (4 entries/event) of events (upper) rejected by, or (lower) after a cut $M(\pi^+\pi^-) < 2.9GeV$

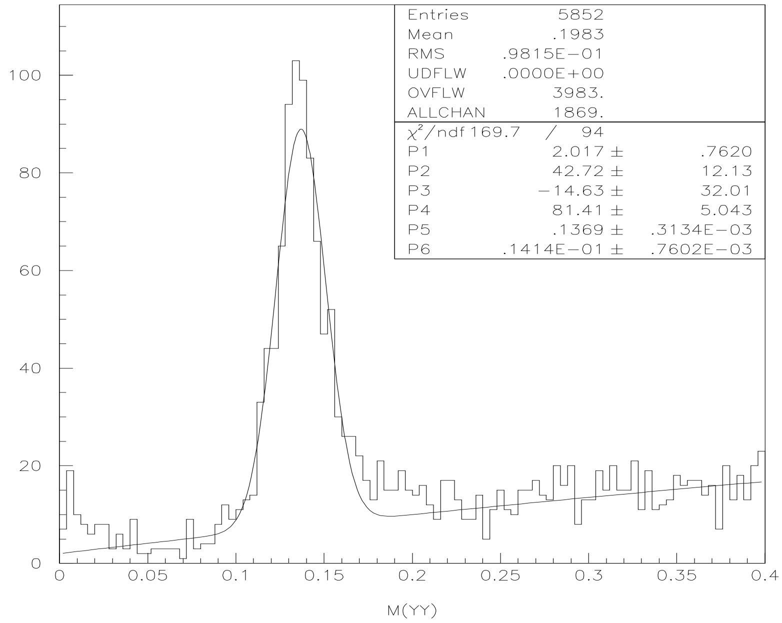

FIG. 4. $M(\gamma\gamma)$ in data $\psi' \to \pi^+\pi^-\pi^+\pi^-\pi^0$

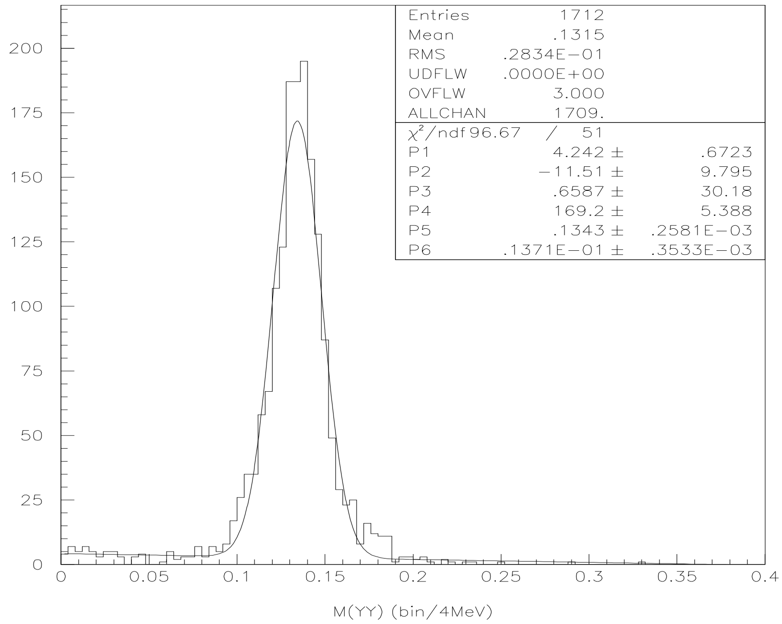

FIG. 5. $M(\gamma\gamma)$ in Monte Carlo $\psi' \to \omega\pi^+\pi^-$

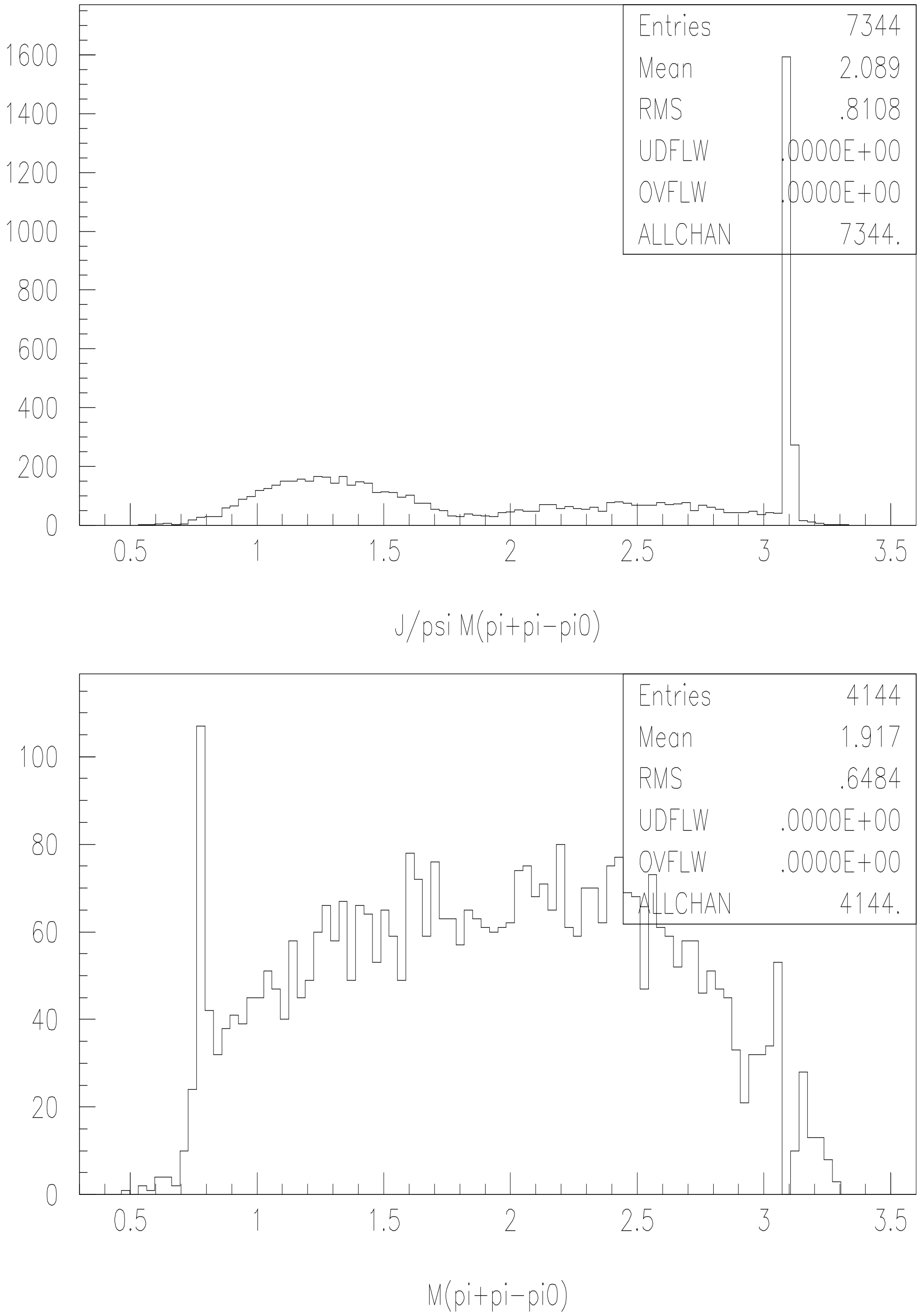

FIG. 6. $M(\pi^+\pi^-\pi^0)$ plot (4 entries/event) for the events (upper) removed as, or (lower) after rejection $\psi(2S) \to \pi^+\pi^- J/\psi$ with $J/\psi \to \pi^+\pi^-\pi^0$.

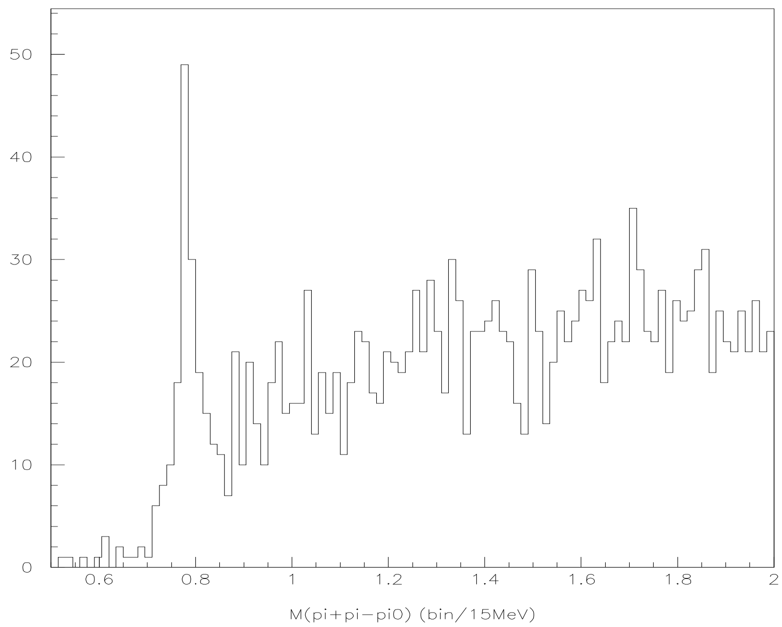

FIG. 7. Mass plot of $\pi^+\pi^-\pi^0$ in $\psi' \to \pi^+\pi^-\pi^+\pi^-\pi^0$

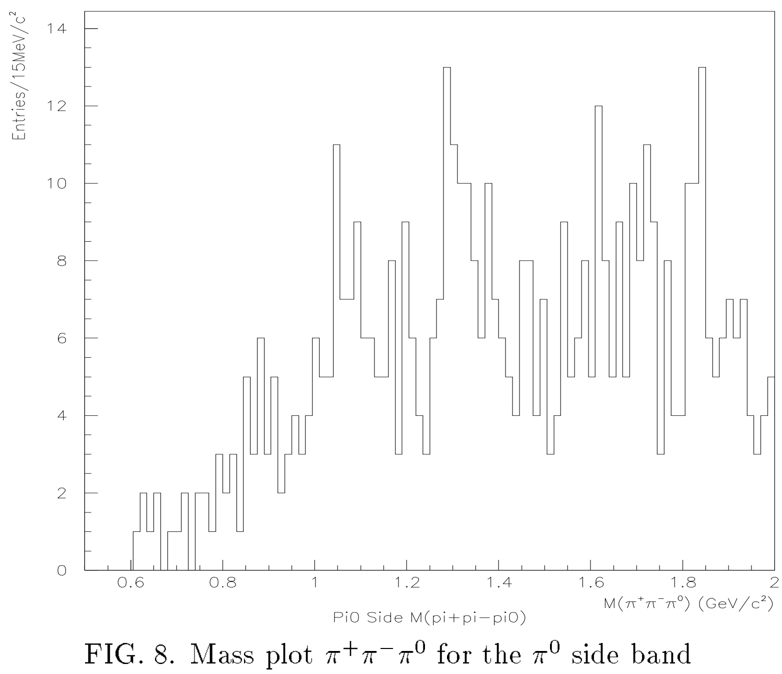

FIG. 8. Mass plot $\pi^+\pi^-\pi^0$ for the π^0 side band

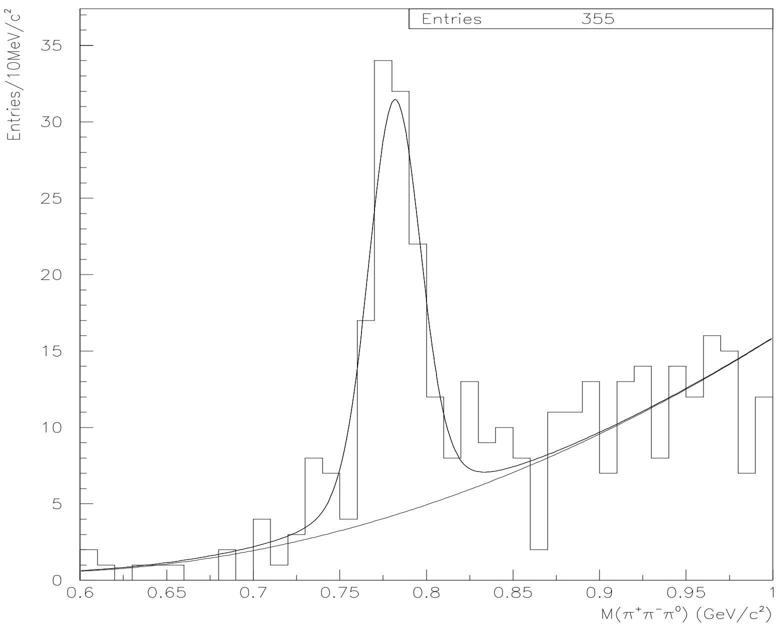

FIG. 9. The ω fit to the $\pi^+\pi^-\pi^0$ mass plot

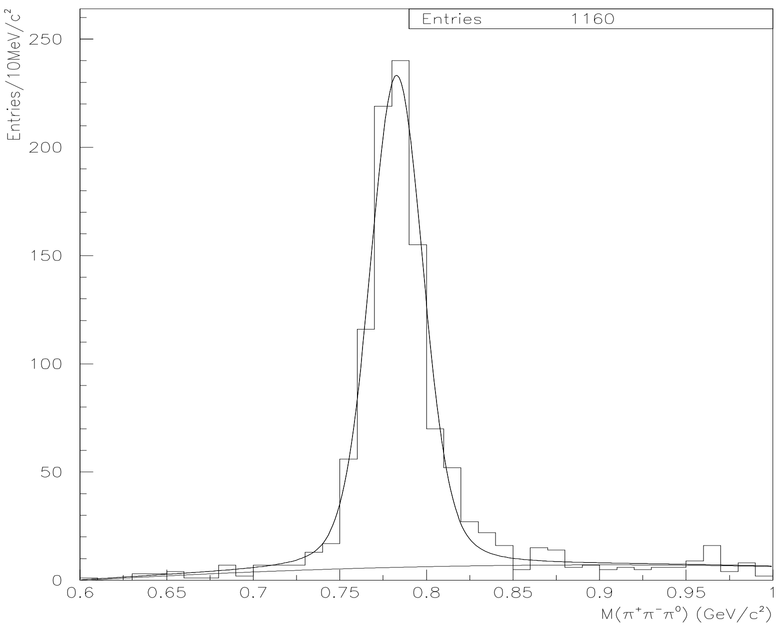

FIG. 10. Fit to the $\pi^+\pi^-\pi^0$ mass plot for the simulation $\psi' \to \omega\pi^+\pi^-$.

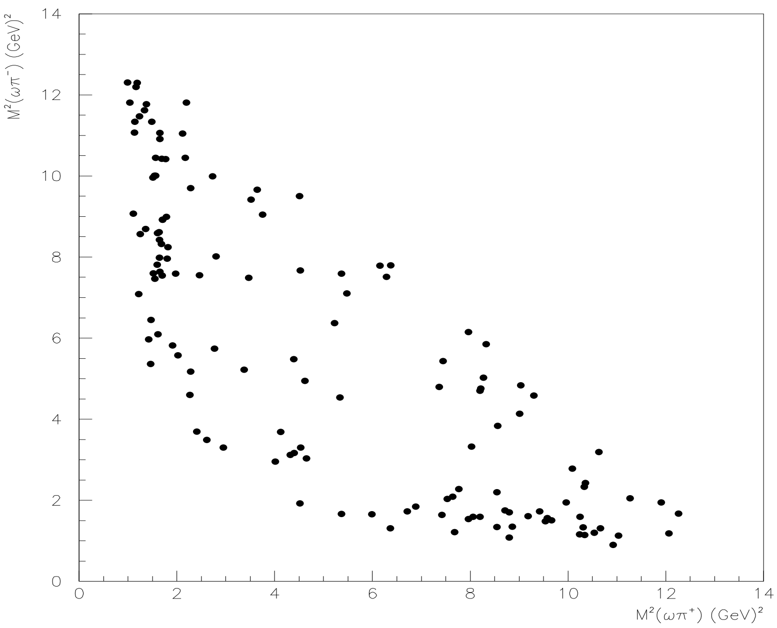

FIG. 11. Dalitz plot of $\omega\pi^+$ vs. $\omega\pi^-$.

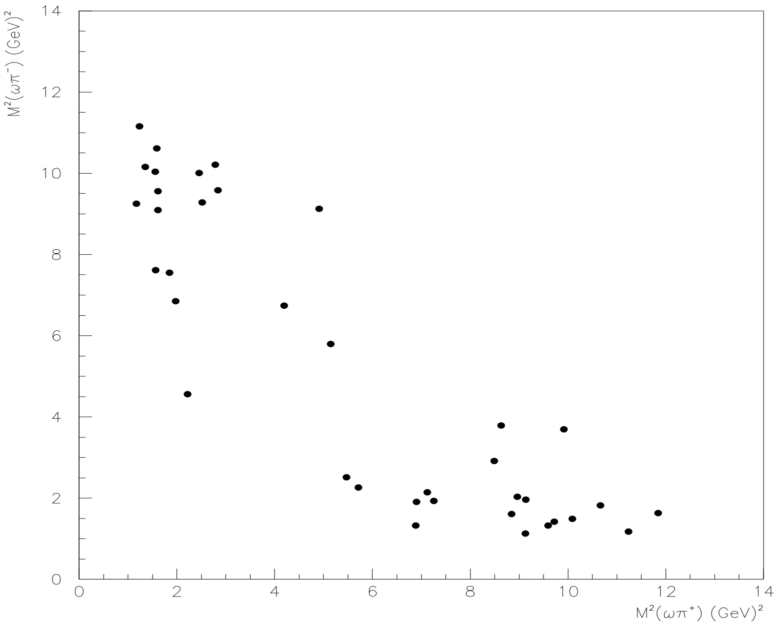

FIG. 12. Dalitz plot of $\omega\pi^+$ vs. $\omega\pi^-$ for ω side band.

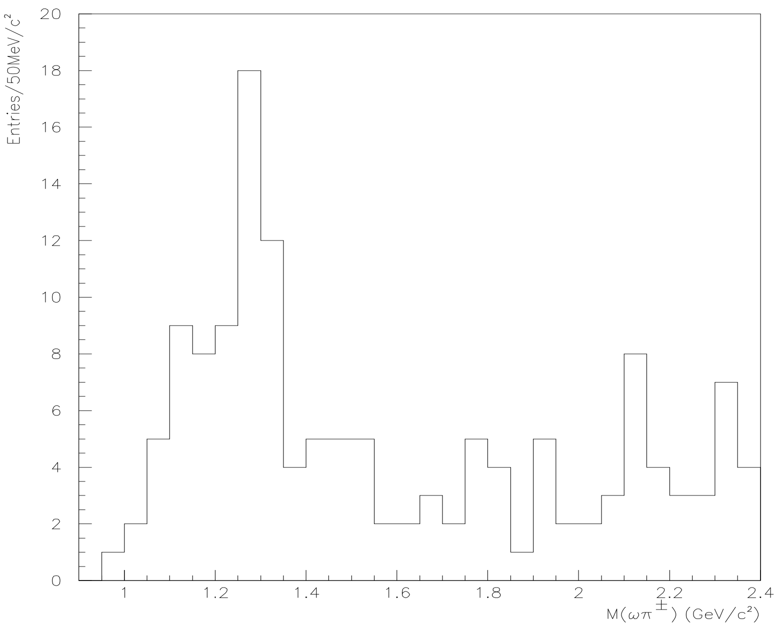

FIG. 13. $\omega\pi^{\pm}$ mass in $\psi' \to \omega\pi^+\pi^-$

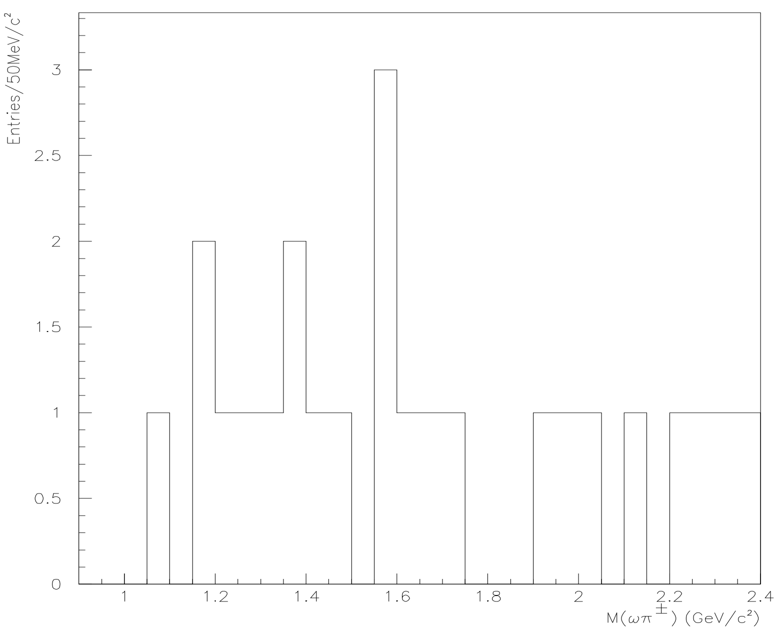

FIG. 14. $\omega\pi^{\pm}$ mass plot for the ω side band.

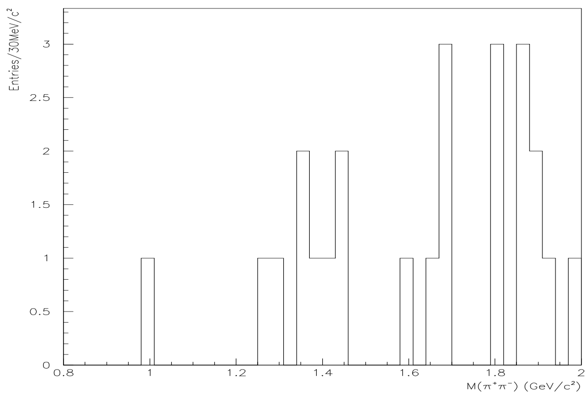

FIG. 15. Mass plot of $\pi^+\pi^-$ recoiling to ω side band

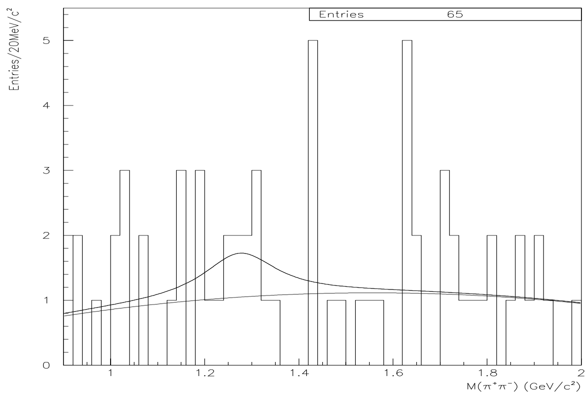

FIG. 16. Fit to plot of $m(\pi^+\pi^-)$ recoiling to ω.

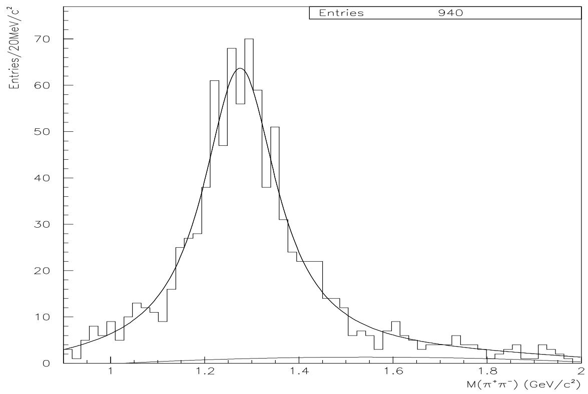

FIG. 17. Fit to plot of $m(\pi^+\pi^-)$ recoiling to ω for the simulation of $\psi' \to \omega f_2$

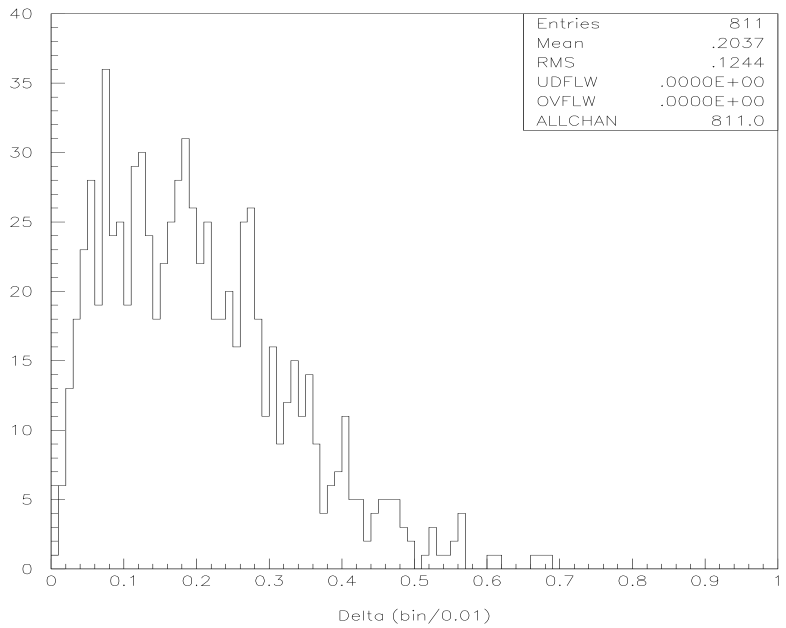

FIG. 18. Δ_{min} plot of data

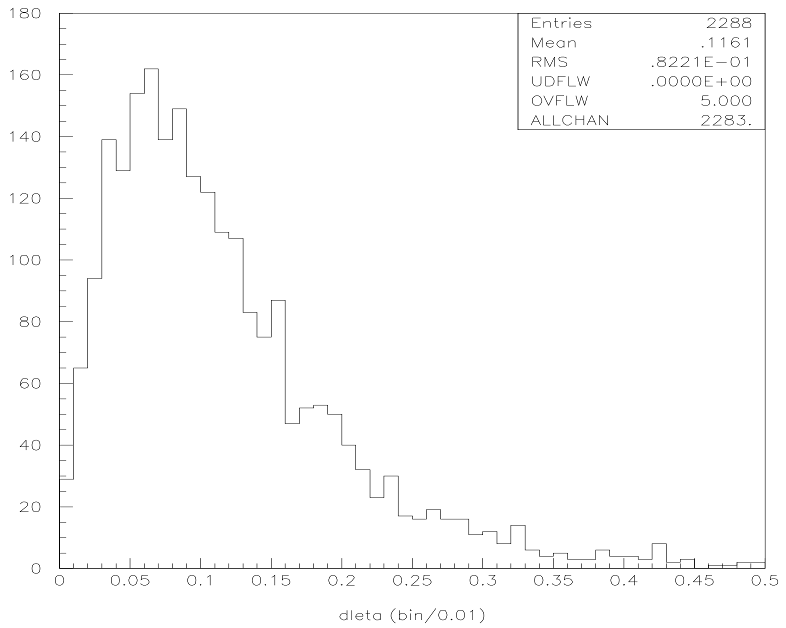

FIG. 19. Δ_{min} plot of the simulation $\psi' \to \rho a_2 \to \rho^0 \rho^{\mp} \pi^{\pm}$

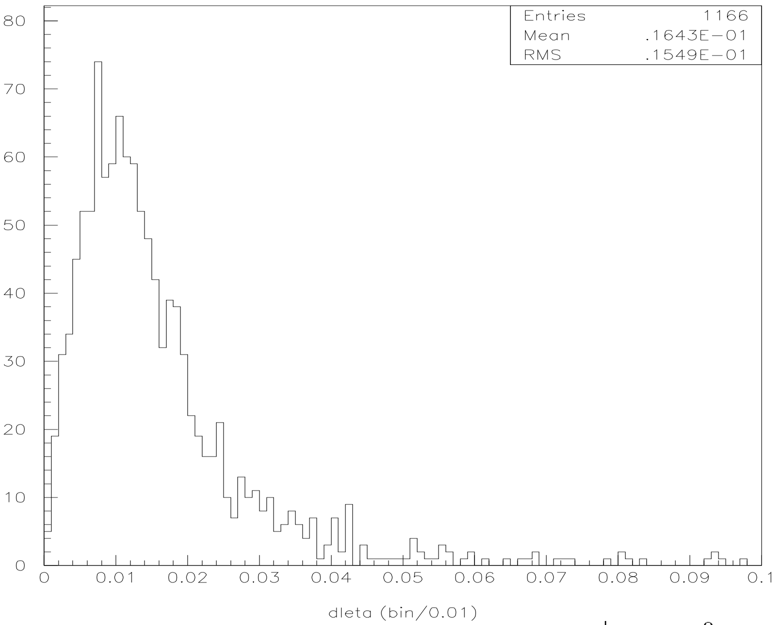

FIG. 20. Resolution plot of Δ_{min} quantity: the widths of $\rho^{\pm}$ and ρ^0 are set to zero in the simulation $\psi' \to \rho a_2 \to \rho^0 \rho^{\mp} \pi^{\pm}$

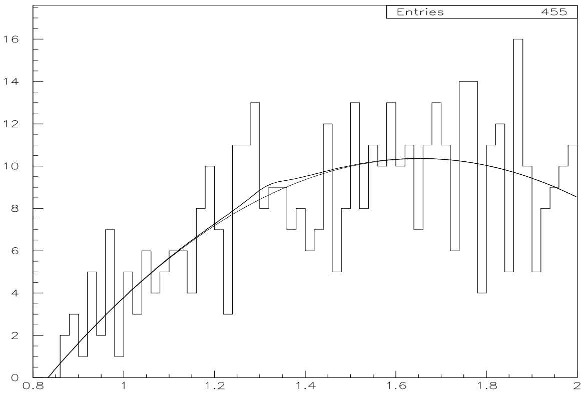

FIG. 21. Fit to plot of $m(\rho\pi)$ in $\psi' \to \rho^0 \rho^{\mp} \pi^{\pm}$

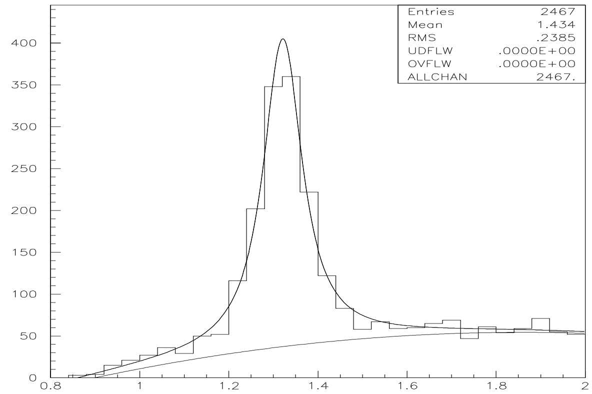

FIG. 22. Fit to plot of $m(\rho\pi)$ in the simulation of $\psi' \to \rho a_2 \to \rho^0 \rho^{\mp} \pi^{\pm}$

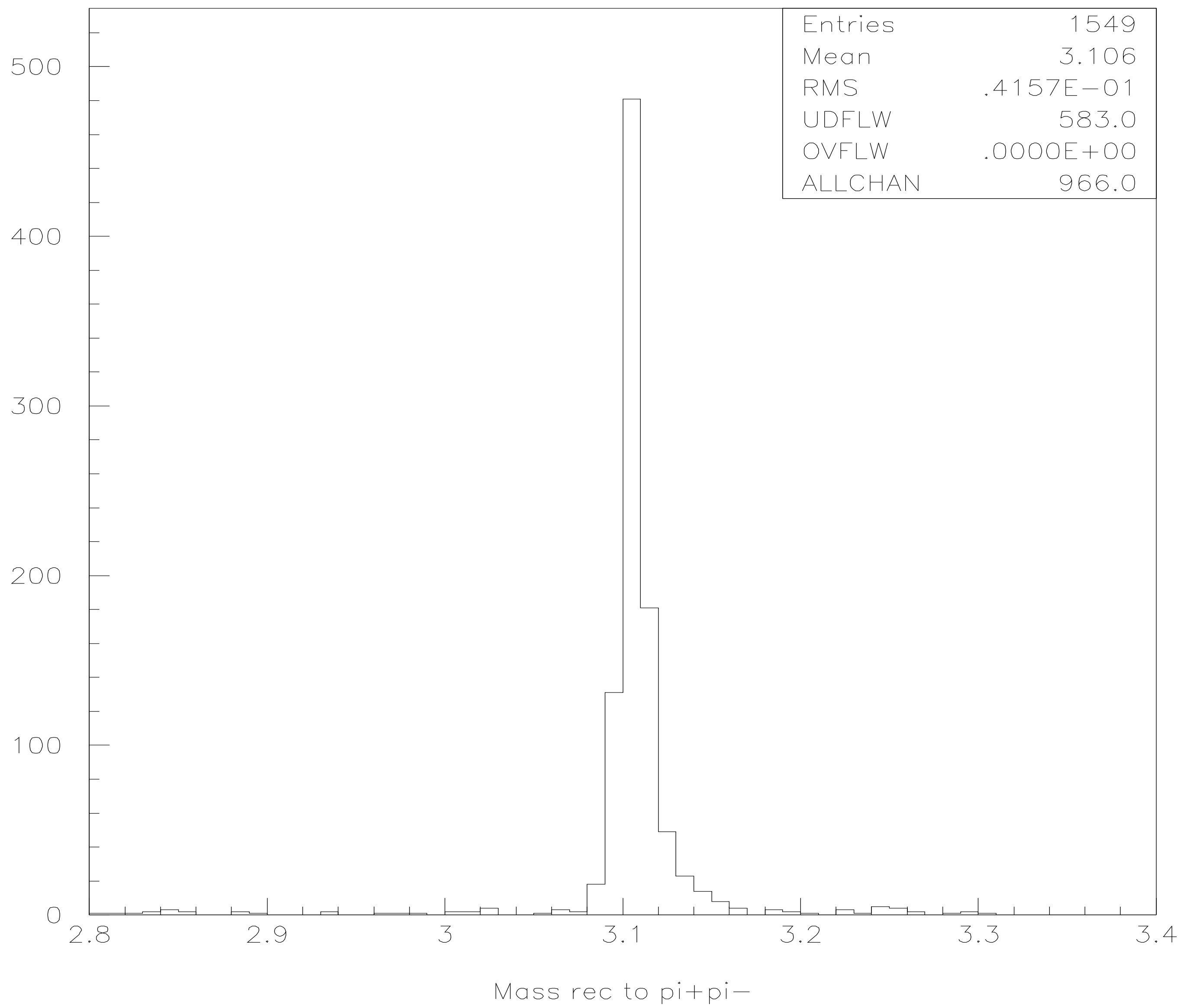

FIG. 23. Mass recoils to $\pi^+\pi^-$ in $\psi(2S) \to \pi^+\pi^- K^+K^-$ analysis.

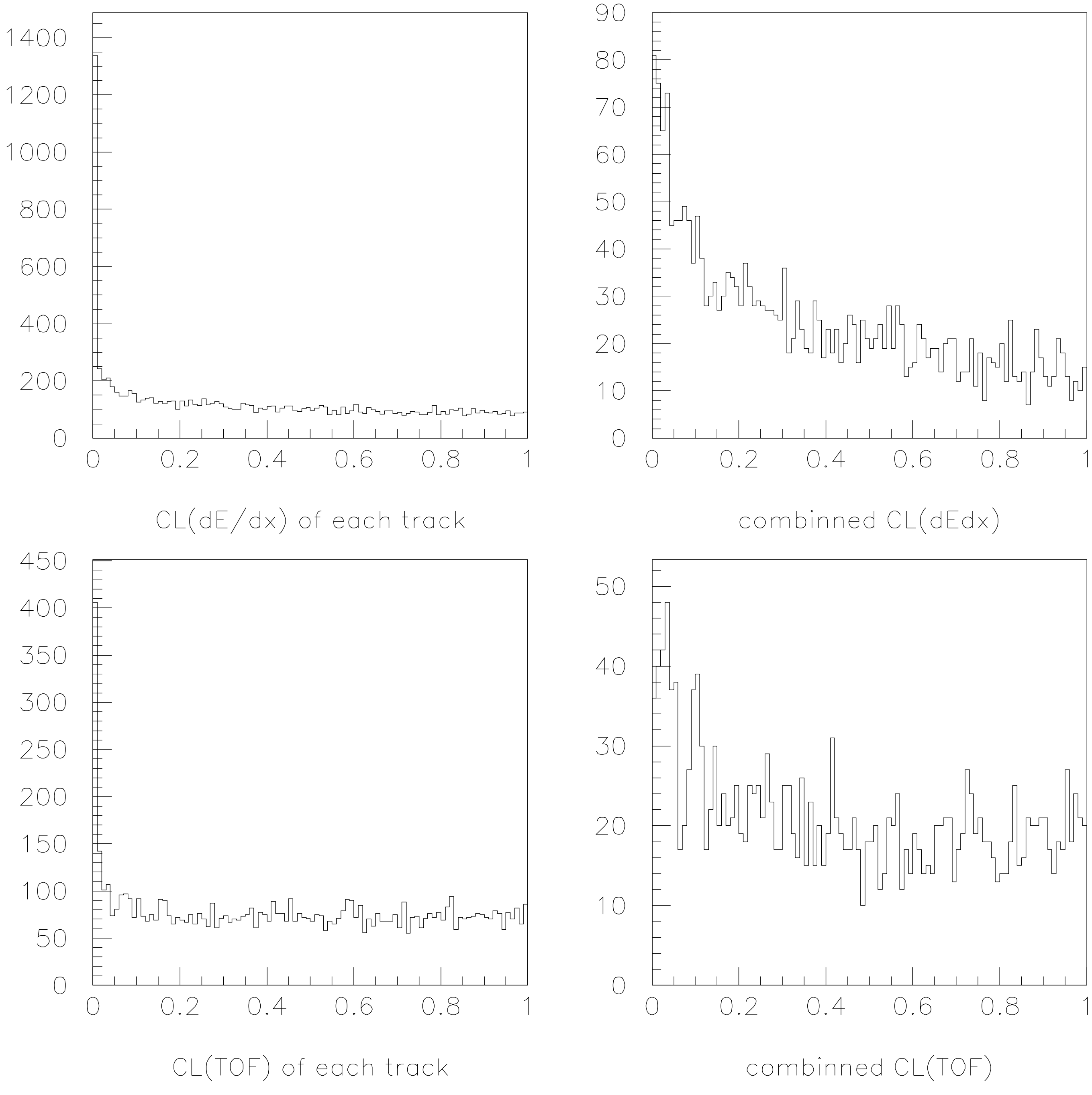

FIG. 24. Confidence level of dE/dx and TOF in $\psi(2S) \to \pi^+\pi^-K^+K^-$ analysis.

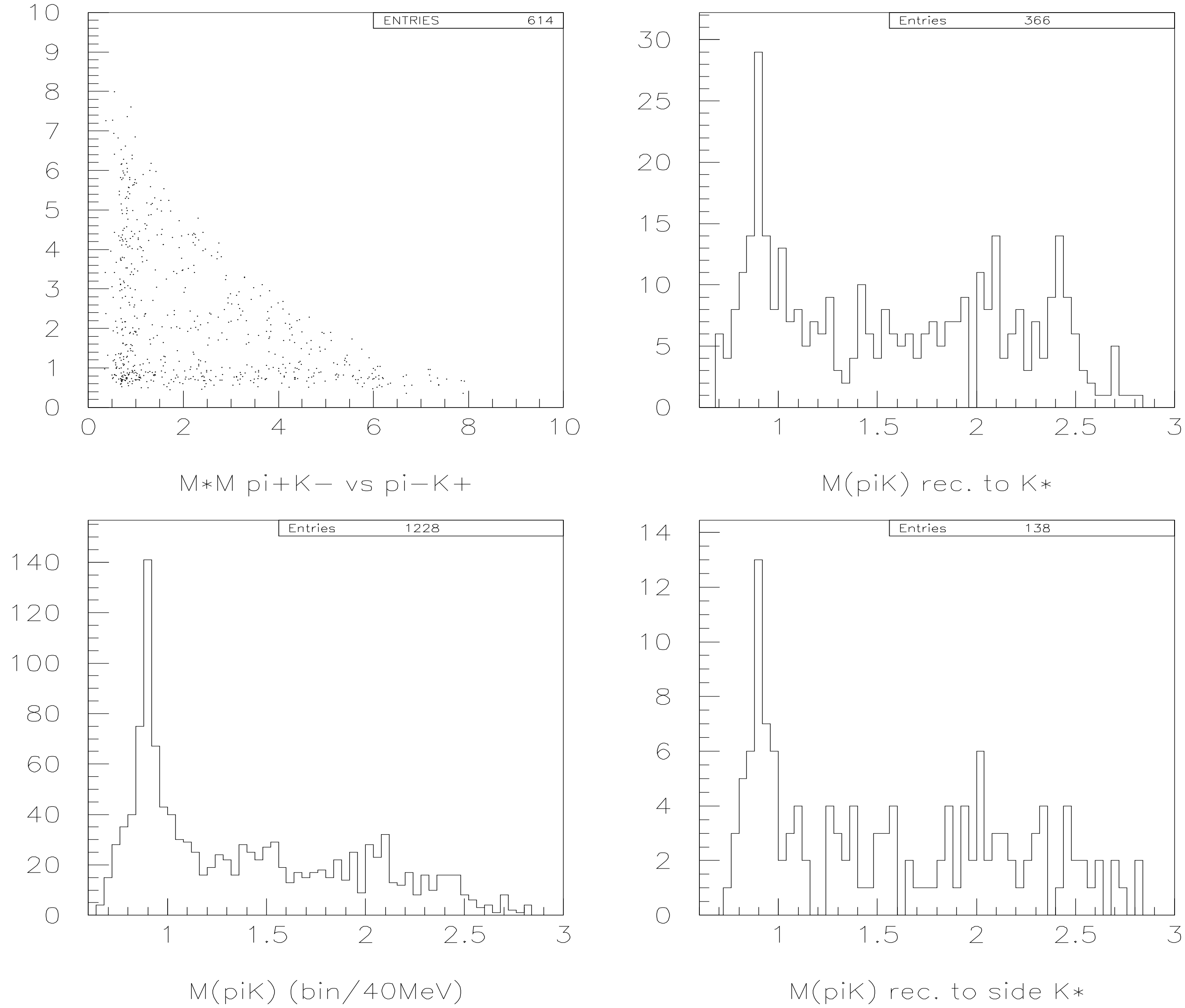

FIG. 25. Plots of $\psi' \to \pi^+\pi^- K^+ K^-$.

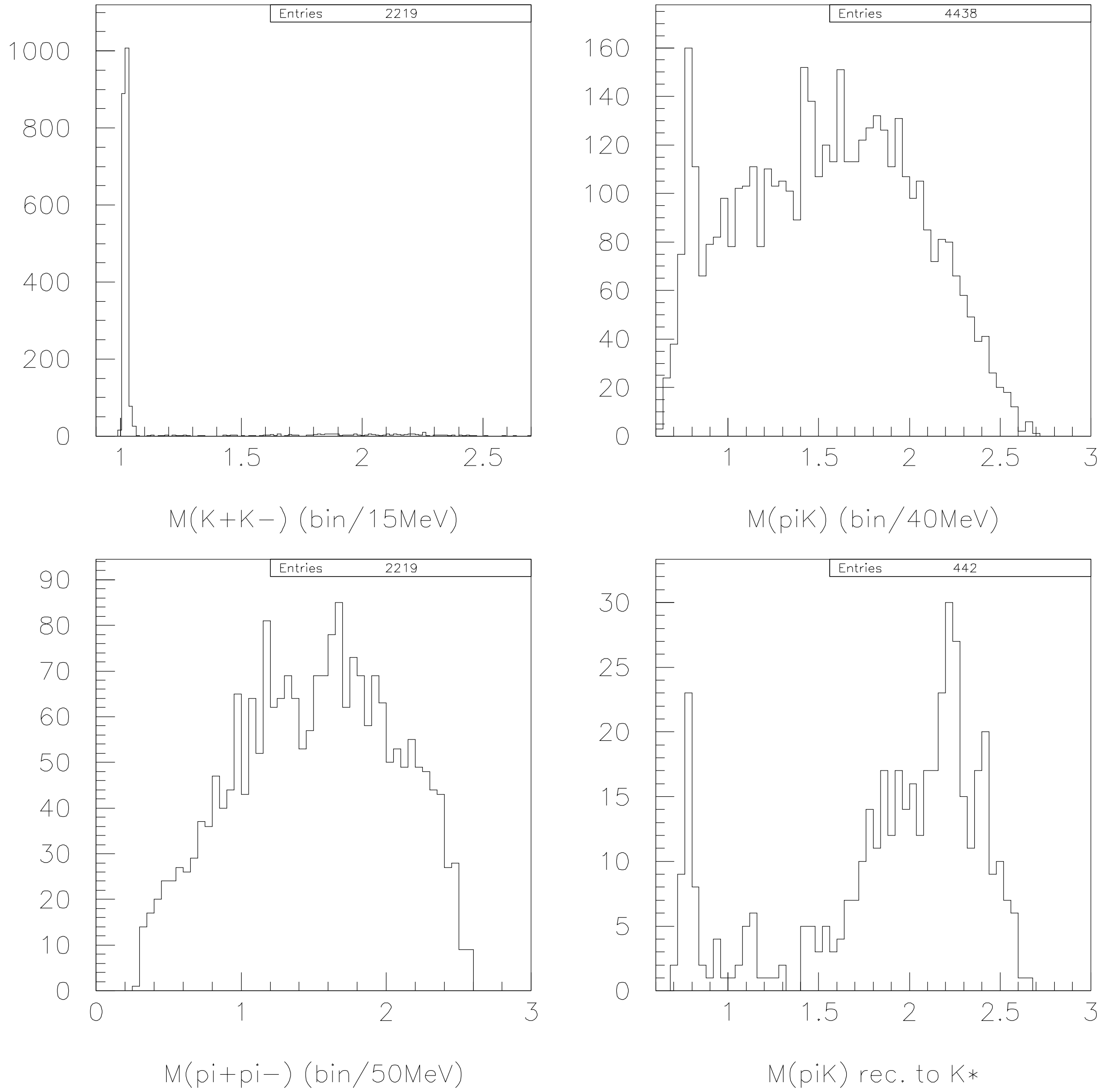

FIG. 26. Plots of simulation $\psi' \to \phi\pi^+\pi^- \to \pi^+\pi^- K^+ K^-$.

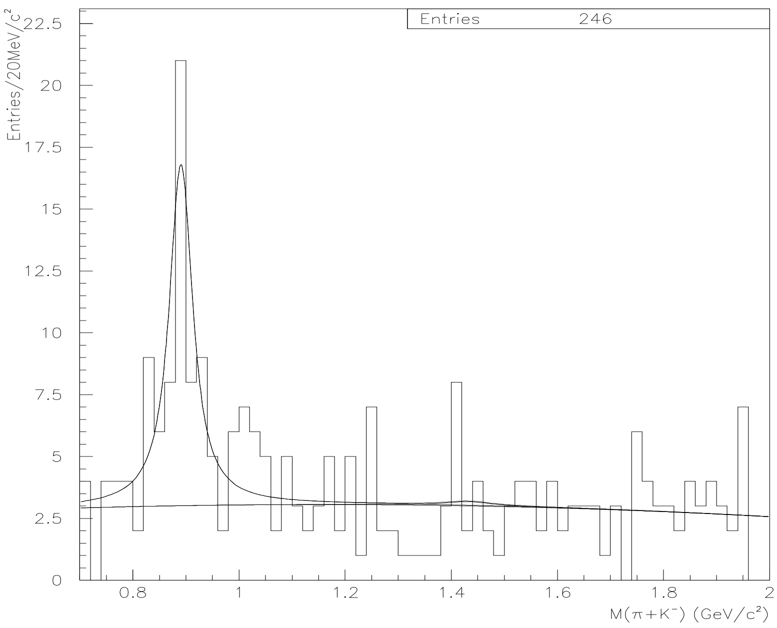

FIG. 27. Fit plot of $m(K^{\pm}\pi^{\mp})$ recoiling to the K^{*0}.

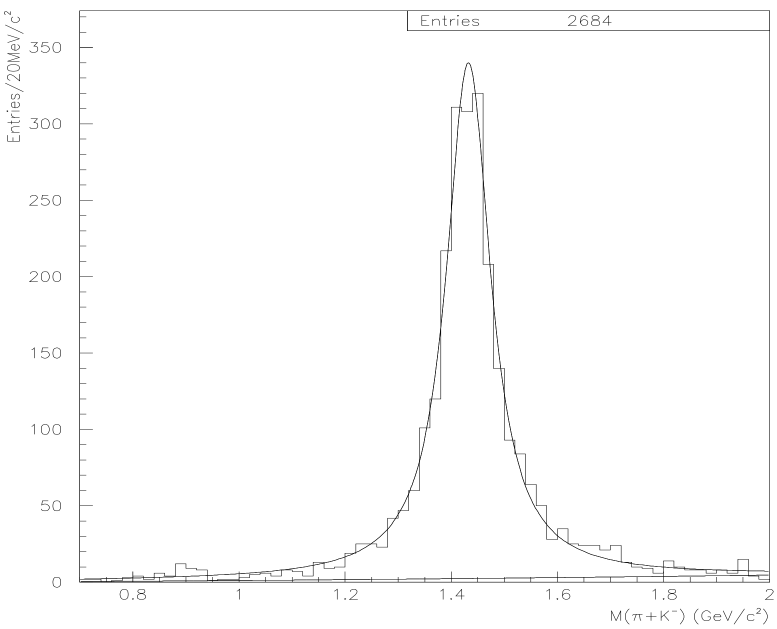

FIG. 28. Fit plot of $m(K^{\pm}\pi^{\mp})$ recoiling to the K^{*0} in Monte Carlo.

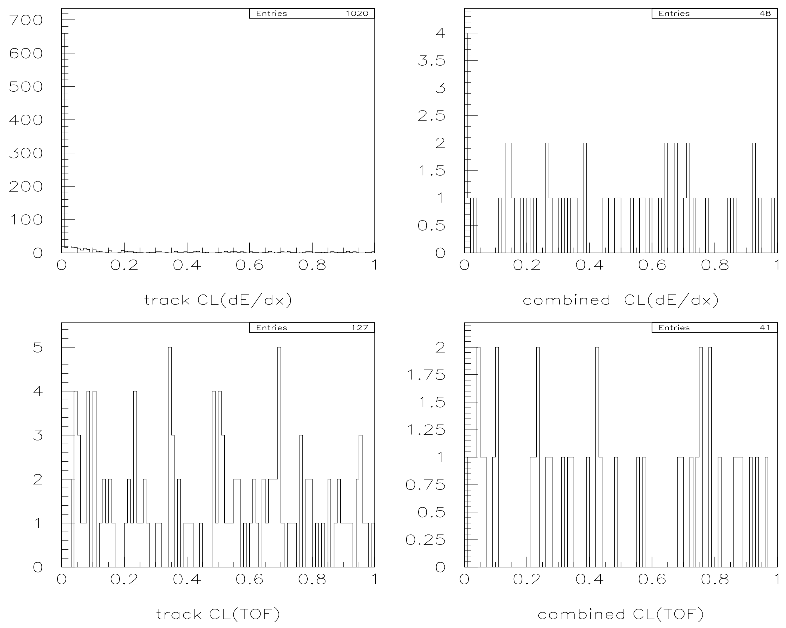

FIG. 29. Confidence level of dE/dx and TOF measurement in $\psi(2S) \to k^+k^-k^+k^-$ selection.

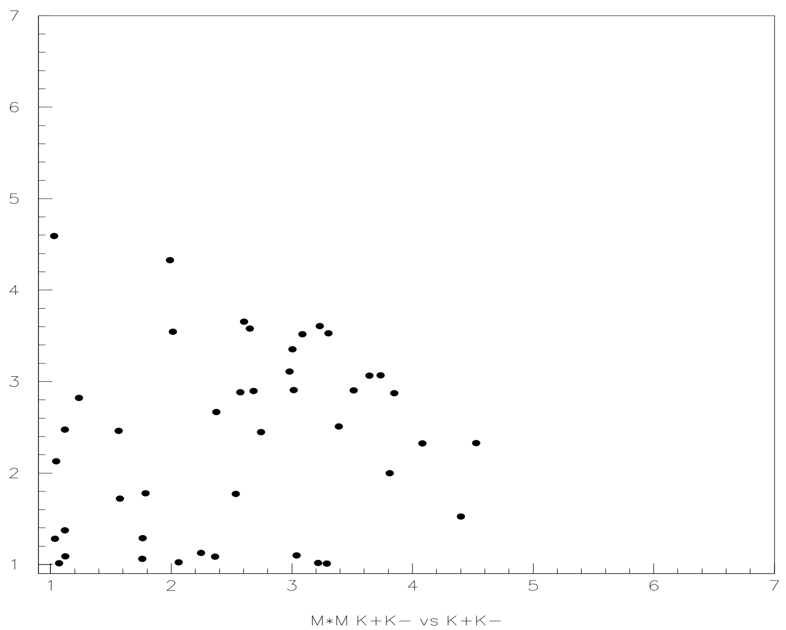

FIG. 30. Dalitz plot in $\psi' \to K^+K^-K^+K^-$

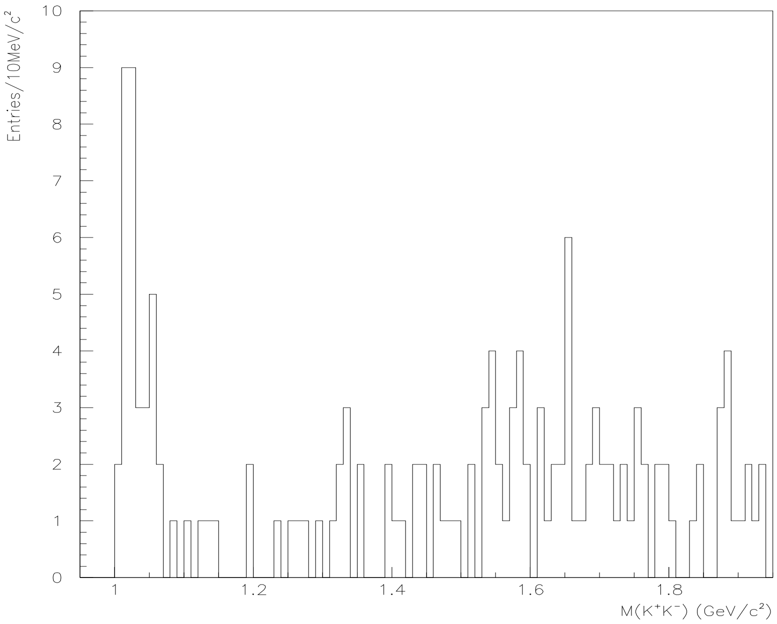

FIG. 31. K^+K^- mass in $\psi' \to K^+K^-K^+K^-$

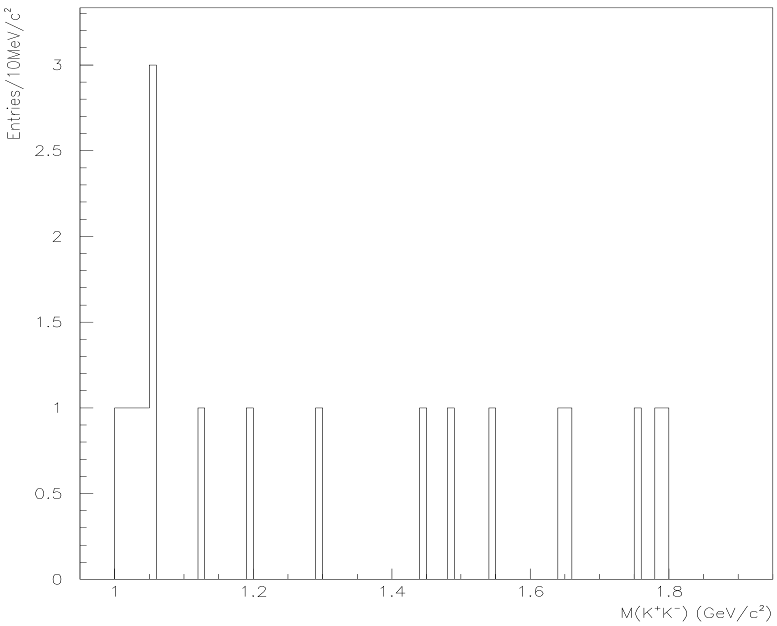

FIG. 32. Mass plot of K^+K^- recoiling to ϕ in $\psi' \to K^+K^-K^+K^-$